


Topological transition from superfluid vortex rings to isolated knots and linksWen-Kai Bai,¹ Tao Yang ^{1,2,3,*} and Wu-Ming Liu ^{4,5,†}¹*Shaanxi Key Laboratory for Theoretical Physics Frontiers, Institute of Modern Physics, Northwest University, Xi'an 710127, China*²*School of Physics, Northwest University, Xi'an 710127, China*³*NSFC-SPTP Peng Huanwu Center for Fundamental Theory, Xi'an 710127, China*⁴*Beijing National Laboratory for Condensed Matter Physics, Institute of Physics, Chinese Academy of Sciences, 100190 Beijing, China*⁵*Songshan Lake Materials Laboratory, Dongguan, Guangdong 523808, China*

(Received 27 March 2020; accepted 24 November 2020; published 16 December 2020)

Knots and links are fundamental topological objects that play a key role in both classical and quantum fluids. In this paper, we propose a scheme to generate torus vortex knots and links through the reconnections of vortex rings perturbed by Kelvin waves in trapped Bose-Einstein condensates, which makes it possible to generate topologically complex structures from topologically trivial objects controllably. The transfer of helicity between knots, links, and coils occur with different pathways which can be controlled through designing specific initial states. The generation of a knot or link can be achieved by setting the parity of the Kelvin wave number. The stability of knots and links can be greatly improved with tunable parameters, including the ideal relative angle and the minimal distance between the initial vortex rings.

DOI: [10.1103/PhysRevA.102.063318](https://doi.org/10.1103/PhysRevA.102.063318)**I. INTRODUCTION**

Knots and links are of great interest in many areas of science including physics, chemistry, and biology. Although they commonly form in nature and everyday occurrences we have all experienced, it is difficult to achieve the controllable formation of these structures with complex topologies. Experimental and theoretical observations of knots and links exhibit highly nonlinear dynamics, which is vital for understanding various persistent phenomena and turbulent behaviors, ranging from water [1,2], superfluid systems [2–9], plasma [10,11], and agitated strings [12] to liquid crystals [13,14], and with increasing importance in a variety of scenarios, such as synthesising DNA and/or RNA in biological systems [15–21] and molecular designing in chemistry [22–25]. In quantum fluids, knots and links are the tangled filaments of vortices. Ultracold atomic Bose-Einstein condensates (BECs) provide a controllable platform for both comprehensive theoretical studies of these topological excitations and direct observations of their dynamics using tunable parameters. The discrete filamentary nature of vortices is an advantage of quantum fluids in studies of vortex interactions and reconnections over ordinary fluids. Due to the similar behaviors that occur in viscous classical fluids and quantum fluids [1,2,4,15,26], it is helpful to understand various persistent phenomena and turbulence in classical fluids by studying the corresponding quantum counterpart.

Great efforts have been made to create knots and links in different classical contexts. For example, isolated trefoil vortex knots and pairs of linked vortex rings were created in

water using a method of accelerating specially shaped hydrofoils produced by 3D printing technology [1], and isolated optical vortex loops in the forms of knots and links were realized by optical beams using algebraic topology [27]. In a recent experiment, a trefoil optical vortex knot was generated through a distribution of single photons [28]. There are also many others, including those in biology and chemistry, to obtain specific functions via different geometric configurations [15–25].

Although it is easy to create structures with trivial topology (vortex rings) or turbulent vortex tangles experimentally, a major challenge is the ability to create nontrivial topologies in a reproducible way. A prototype structure with relative simple nontrivial topology is clearly the torus knot. Unfortunately, attempts to create reproducible knots by colliding vortex rings have not been successful [29]. Moreover, most of the theoretical studies focus on the dissolving of knots and links [2,4,7,20,30–33] or head-on collisions [34,35], where only standard reconnections occur. In this process, the reduced complexity of the topological structures is identified through stepwise reduction, which shows the transfer of helicity of the system evolves only in one direction from knotted (linked) structures to helical coils [4,36]. In most cases, topological complex structures will decay into simpler ones [4,7,8], but the opposite process has also been observed in turbulent tangles [29,37].

It was found that reconnecting vortex lines generally separate faster than they approach, leading to the irreversibility of the reconnection events [33,38,39]. The linear momentum and energy exchanges between the incompressible (vortices) and compressible (density waves) degrees of freedom of the superfluid were determined quantitatively for a better understanding of the mechanism of vortex reconnection in quantum fluids [33,38]. Kelvin modes have reported direct evidence in

*yangt@nwu.edu.cn

†wmliu@iphy.ac.cn

a single-vortex BEC [40,41]. During the reconnection process, cusps are generated and the vortex lines are excited by Kelvin waves, helical perturbations that travel along the vortices, as they relax [42,43]. In turn, the Kelvin waves provide a source of perturbations for the motion of vortices. The Kelvin wave cascade generated in superfluid turbulence reflects the importance of Kelvin waves and reconnections in the transfer of energy [42], which may be exploited to stabilize vortex structures. The knot and link dynamics with Kelvin perturbations in confined systems remains a topic of research. The objective of our study is to make the reconnections of vortices occur controllably and then form the complex structures wanted in BECs. Generally, condensates are confined in magneto-optical traps experimentally, which are suitable for exploring systems with different geometries. In the main text, we consider harmonically trapped systems as examples. The systems with box-trapping potentials and periodic boundary conditions are discussed in Appendixes D and E, respectively.

II. MODEL FOR NUMERICAL SIMULATIONS

To achieve the goal of generating knots and links, we use topologically trivial objects, that is, vortex rings in a spherical BEC, as building blocks. A vortex ring is a stable nonlinear excitation mode that can be simply described as a vortex line that has been bent into a closed loop. In a trapped BEC, a vortex ring moves in response to the effect of the nonuniform trap potential and the external rotation, in addition to self-induced effects caused by the local curvature of the ring [44]. By introducing Kelvin waves into the system, the vortex ring is modified by periodic distortions, which reduces the translational self-induced velocity of the vortex ring [45,46] and adds helicity to the vortex ring. In ideal fluids, which lack viscosity, helicity [47] is a conserved quantity that measures the degree of knottedness and entanglement of a fluid flow. Helicity can be stored by twisting, writhing (coiling and knotting), and linking [11]. In quantum fluids, helicity varies with topology-changing reconnections and changes of geometry in helical vortices. We discuss the evolution of helicity in detail in Appendix A.

The interaction between vortices is another factor that plays an important role in vortex dynamics and leads to interesting phenomena. In homogeneous systems, one of the most impressive sights occurs when two same-sized vortex rings placed front to back move together in the same direction by leapfrogging through each other [48]. When one of the rings is helically wound initially, the centerline helicity varies considerably, and the leapfrogging motion occurs due to the stretching and compressing of the helical ring [2,26]. However, the reconnections do not occur between these independent rings.

At sufficiently low temperatures, the macroscopic behavior of a trapped BEC with N atoms is well characterized by the Gross-Pitaevskii (GP) equation, which is useful for studying topological vortex excitations,

$$i\hbar \frac{\partial \psi}{\partial t} = \left(-\frac{\hbar^2}{2m} \nabla^2 + V_{\text{tr}}(\mathbf{r}) + g|\psi|^2 \right) \psi, \quad (1)$$

where ψ is the wave function, the coupling constant $g = 4\pi \hbar^2 a_s/m$ is related to the s -wave scattering length a_s of the

atoms, and m is the mass of the atoms. In this study, we use an isotropic harmonic trap $V_{\text{tr}}(\mathbf{r}) = m\omega^2 \mathbf{r}^2/2$, where ω is the trap frequency. The oscillation length of the trap and unit of time are $a_0 = \sqrt{\hbar/m\omega}$ and $t_0 = 1/\omega$, respectively.

In our simulations, the isotropic trap frequency is $\omega = 2\pi \times 75$ Hz. The bulk s -wave scattering length is $a_s = 5.4$ nm and the mass $m = 1.443 \times 10^{-25}$ kg for the ^{87}Rb BEC. We use $a_0 = \sqrt{\hbar/m\omega}$ and $t_0 = 1/\omega$ as the units of length and time, respectively. In the calculations, $151 \times 151 \times 151$ grids with steps $\Delta_x = \Delta_y = \Delta_z = \sqrt{2}a_0/10$ are used in a uniformly discretized physical space. A small time step, $\Delta_t = 0.001t_0$, is chosen to ensure the accuracy of the results. The characteristic radius (Thomas-Fermi radius) of the BEC cloud $R_{\text{TF}} = \sqrt{2\mu_{\text{TF}}/m\omega^2}$, where $\mu_{\text{TF}} = (15a_s \hbar^2 \sqrt{m\omega^3 N_0})^{2/5}/2$ is the corresponding chemical potential with N_0 being the number of atoms. As the healing length ξ takes its minimum value at the point of the highest density, one can get $\xi = \hbar/\sqrt{2m\mu_{\text{TF}}}$ under Thomas-Fermi approximation. For the parameters employed in this work, we have $R_{\text{TF}}/\xi = 33.50$. The temporal evolution of the superfluid order parameter was computed by numerically integrating the GP equation using the Crank-Nicolson method and fourth-order Runge-Kutta method, which give quantitative agreement.

In a spherically trapped condensate, two unperturbed vortex rings of similar size can undergo a leapfrogging motion back and forth without reconnections. This process occurs when only one vortex ring is perturbed by Kelvin waves. In a trapped condensate, when the minimum distance between the vortices reaches the order of the Thomas-Fermi radius R_{TF} for the shortest direction in the condensate, the vortices start to rotate to arrange themselves in an antiparallel orientation, followed by reconnection in a direction orthogonal to their mutual alignment before final separation [43,49]. This process is a general characteristic of reconnection events, even in DNA biology [19,50]. The initial relative orientation and velocity of the vortex lines are crucial factors that influence the evolution of the vortices in a trapped condensate [43,51]. The objective of the study is to create knots or links of different topological types in a trapped condensate. Thus, we begin with two separated vortex rings perturbed by helical Kelvin waves of a given amplitude and azimuthal wave number to ensure that reconnections occur.

We label links and knots using the generalized method proposed by Scott and Dror called Knot Atlas [52]. The first topologically nontrivial knot is the trefoil knot K3-1 with a crossing number and topological writhe of $n_c = 3$ and $n_w = 3$, respectively. For links, the second nontrivial link is Solomon link L4a1 with $n_c = n_w = 4$. In the following paragraph, we use these two topological structures as examples to describe our scheme for generating knots and links with different topologies.

A vortex ring is formed by a loop in a vortex line. Suppose that a vortex ring is initially placed on the xOy plane and symmetrically rotated about the z axis; in this case, it can be considered as an assembly of 2D vortex dipoles in the rOz plane. A sufficiently accurate description of a two-dimensional vortex centered at the origin of the rOz plane can be given by the wave function $\psi_{2\text{D}}(r, z) = \sqrt{\rho(l)} \exp[i\theta(r, z)]$, with $\rho(l) = l^2(a_1 + a_2 l^2)/$

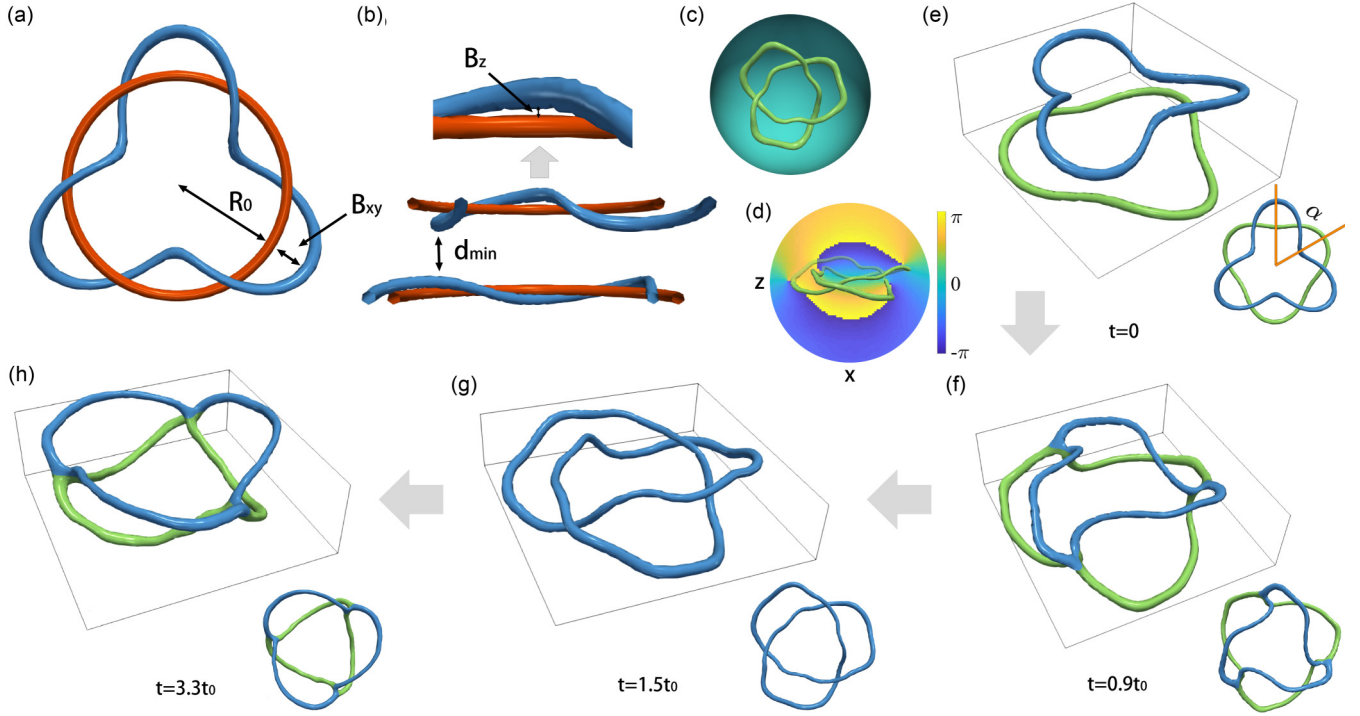


FIG. 1. Initial state and geometric evolution from vortex rings to a trefoil vortex knot. (a), (b) Schematic diagram of a vortex ring perturbed by Kelvin waves with wave number $n = 3$. The unperturbed red ring is used as a reference. (c), (d) Example of the density isosurface of a trefoil vortex knot in a spherical condensate and a cross section of the corresponding phase distribution. (e)–(h) Four successive typical snapshots that show how two distorted vortex rings tie into a K3-1 trefoil vortex knot and then break up again. The trefoil vortex knot emerges at $1.0t_0$ and decays at $3.2t_0$. The initial radii and the minimal distance of the upper and lower vortex rings are $R_1 = 2.0a_0$, $R_2 = 2.3a_0$, and $d_{\min} = 1.0a_0$, respectively. The amplitudes of the Kelvin waves for the upper ring are $B_{xy1} = 0.8a_0$ and $B_{z1} = 0.3a_0$, and for the lower ring, $B_{xy2} = 0.4a_0$ and $B_{z2} = 0.2a_0$. The initial relative angle between the rings is $\alpha = \pi/3$, as shown in (e).

$(1 + b_1 l^2 + b_2 l^4)$, $\theta(r, z) = \text{atan2}(z, r)$, $r = \sqrt{x^2 + y^2}$, and $l = \sqrt{r^2 + z^2}$, where a_j and b_j are constants, and $\text{atan2}(\dots)$ is the extension of the arctangent function with a principal value in the range of $(-\pi, \pi]$. The vortex rings modified by Kelvin waves with periodic distortion can be initialized by a three-dimensional wave function [7,8,46],

$$\begin{aligned}
 \psi_{3D}(x, y, z) = & \psi_{2D}\{r - R_1 - B_{xy1}\sin[n\theta(x, y) + n\alpha], \\
 & \times z - Z_0 - B_{z1}\cos[n\theta(x, y) + n\gamma]\} \\
 & \times \psi_{2D}^*\{r + R_1 - B_{xy1}\sin[n\theta(-x, -y) + n\alpha], \\
 & \times z - Z_0 - B_{z1}\cos[n\theta(-x, -y) + n\gamma]\} \\
 & \times \psi_{2D}\{r - R_2 - B_{xy2}\sin[n\theta(x, y)], \\
 & \times z + Z_0 - B_{z2}\cos[n\theta(x, y)]\} \\
 & \times \psi_{2D}^*\{r + R_2 - B_{xy2}\sin[n\theta(-x, -y)], \\
 & \times z + Z_0 - B_{z2}\cos[n\theta(-x, -y)]\}, \quad (2)
 \end{aligned}$$

where B_{xyj} and B_{zj} ($j = 1, 2$) are the amplitudes in the radial and axial directions of the Kelvin waves applied for the j th vortex ring, respectively, and n is the wave number of the Kelvin wave perturbations for both rings. The initial rotation of the upper vortex ring around the z axis is given by α , and γ is the angle of inclination with respect to the unperturbed ring. Then, the minimal offset between the two rings is $d_{\min} = 2Z_0 - B_{z1} - B_{z2}$. The symmetrical placement of the two coaxial rings with respect to the xOy -plane results in n

pairs of points between the two rings with the same distance d_{\min} .

In superfluid systems without fluctuations, the reconnection of those points with a minimum distance occurs simultaneously. In Ref. [2], the simultaneous reconnections during the dissolution of knots reduced the complexity of the topology. In Ref. [4], distortions were applied to knots and links, and simultaneous reconnections were avoided during the untying process.

Figures 1(a) and 1(b) show the relevant parameters for perturbing a vortex ring using helical Kelvin waves, where R_0 is the radius of the unperturbed ring, shown in red; B_{xy} and B_z are the amplitudes of the Kelvin perturbations in the xOy plane and z direction, respectively; and d_{\min} is the minimal initial offset between the two rings along the propagation axis. If d_{\min} is not specially given, we set $d_{\min} = a_0$. The relative angle α between the rings is shown in the subplot of Fig. 1(e). Two perturbed rings with radii less than the equilibrium radius [53] and the same winding number move in the same direction. The equilibrium radius can be reached when the precession due to the inhomogeneity of the condensate is balanced by the induced velocity resulting from the sum of the velocity contributions from each element on the vortex ring. A vortex ring with an equilibrium radius is in an unstable equilibrium state where there is no relative motion between the ring and the condensate cloud [53,54]. The advantage of this system is that it has a well-controlled initial state that can be created within a spatially confined region and reconnection occurs

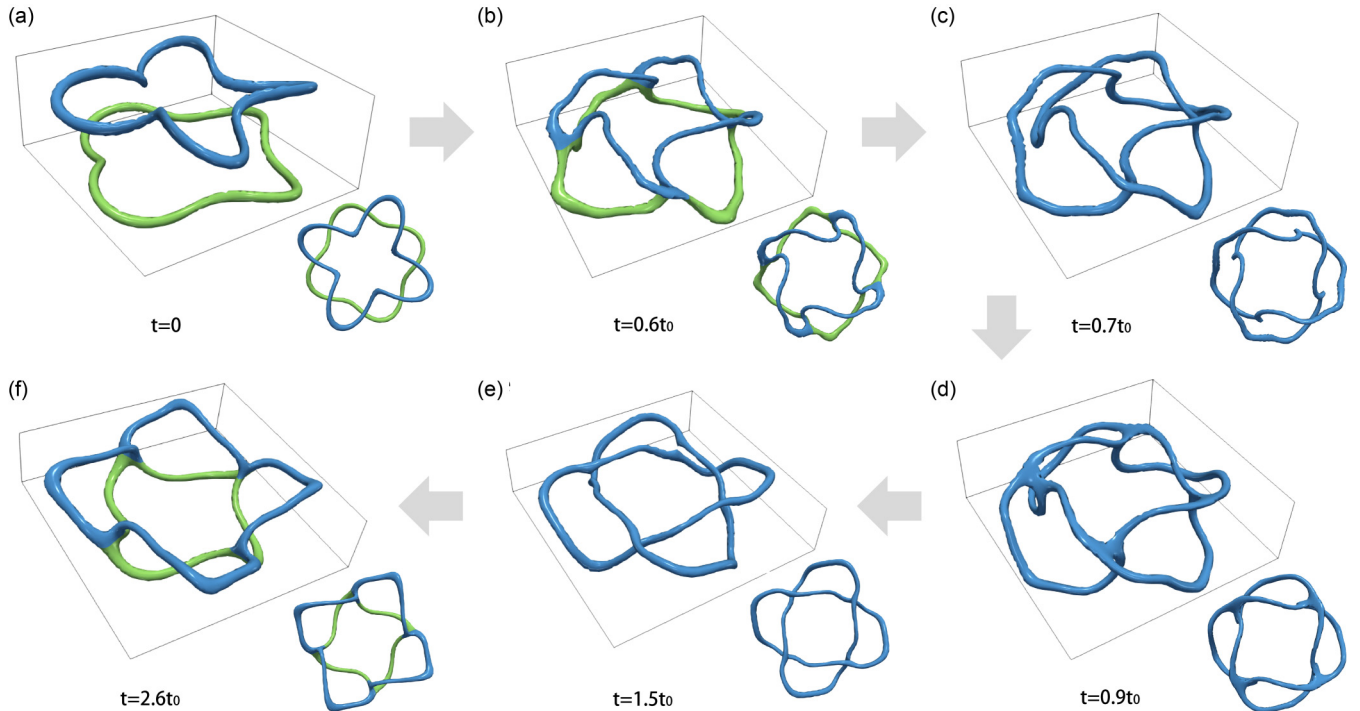


FIG. 2. Generation of a L4a1 Solomon vortex link. (a)–(f) Six successive snapshots that show how two perturbed vortex rings with Kelvin wave number $n = 4$ evolve into the L4a1 vortex link and then break up again. The link appears twice between $0.7t_0$ and $0.8t_0$ (c) and between $1.1t_0$ and $2.5t_0$ (e). All other parameters are the same as those in Fig. 1.

naturally due to the different velocities and perturbations of the vortex rings. In addition, the initial parameters can be easily adjusted, which allows us to study the stability of the knots and links generated. Figures 1(c) and 1(d) show the isosurface and corresponding phase distribution of the trefoil structure in our system as an example.

III. RESULTS

A. Generation of a trefoil knot

To generate a trefoil structure, the rings are initially perturbed by helical Kelvin waves with an odd wave number, $n = 3$, copropagating in the z direction in our system. Simulations are performed with the initial radii of the vortex rings set to $R_1 = 2a_0$ (blue radius at the top) and $R_2 = 2.3a_0$ (green radius at the bottom), as shown in Fig. 1(e), and the initial positions of the two rings in the z direction are $z = 0.75a_0$ and $z = -0.75a_0$, respectively. We note that the ranges of the radii of the initial vortex rings are limited because small rings cannot resolve the sound pulse and large rings require many grid points [55]. By chosen appropriate parameters, we ensure that the top ring has a higher velocity than the bottom ring, which is an important factor for the association of the two rings. We note that the interaction between rings dominates in our system configuration.

A typical time sequence that illustrates the collision and connections of the initial unlinked vortex rings in Figs. 1(f)–1(h) shows some typical topological structures that form during the evolution. As the radii of the rings stretch and shrink during the movement of the rings along the z axis, the top ring catches up with the bottom ring, and connections occur at approximately $t = 0.9t_0$ via three simultaneous

reconnection events, as shown in Fig. 1(f). A trefoil knot K3-1 with a clear structure and propagation direction identical to that of the initial unlinked rings appears in the condensate cloud, as shown in Fig. 1(g). The trefoil knot exists in the $z < 0$ space from $t = 1.0t_0$ to $t = 3.2t_0$. At approximately $t = 3.3t_0$, the knot breaks up via three simultaneous self-reconnection events, as shown in Fig. 1(h), before decaying into two independent rings. In this case, the bridge structures in Figs. 1(f)–1(h) are formed through topology-changing reconnections, which alter the topology of the system. In Supplemental Movie1-K3-1.mp4 [56], we show the time evolution of the vortex structures with another set of initial parameters which make the trefoil knot exist longer.

B. Generation of a Solomon link

If the wave number of Kelvin waves is chosen to be an even number, $n = 4$, the vortex link L4a1 (Solomon link) is generated via collisions and reconnections of the unlinked vortex rings as shown in Fig. 2. All the other initial conditions are the same as those used in Fig. 1 a. During evolution, the rings perturbed by Kelvin waves distort and reconnect at approximately $t = 0.6t_0$, as shown in Fig. 2(b). In Fig. 2(c), we show that at $t = 0.7t_0$, the link L4a1 is generated in the trapped condensate for the first time after the free evolution of the initial rings. However, the link configuration is unstable, and another reconnection event occurs at $t = 0.9t_0$, as shown in Fig. 2(d). Then, the bridge structure evolves into a vortex link at $t = 1.5t_0$, and this link survives much longer than the previous one; another bridge structure appears at $t = 2.6t_0$, as shown in Fig. 2(f), and then unties to form two highly distorted vortex rings (also see Supplemental Movie2-L4a1.mp4

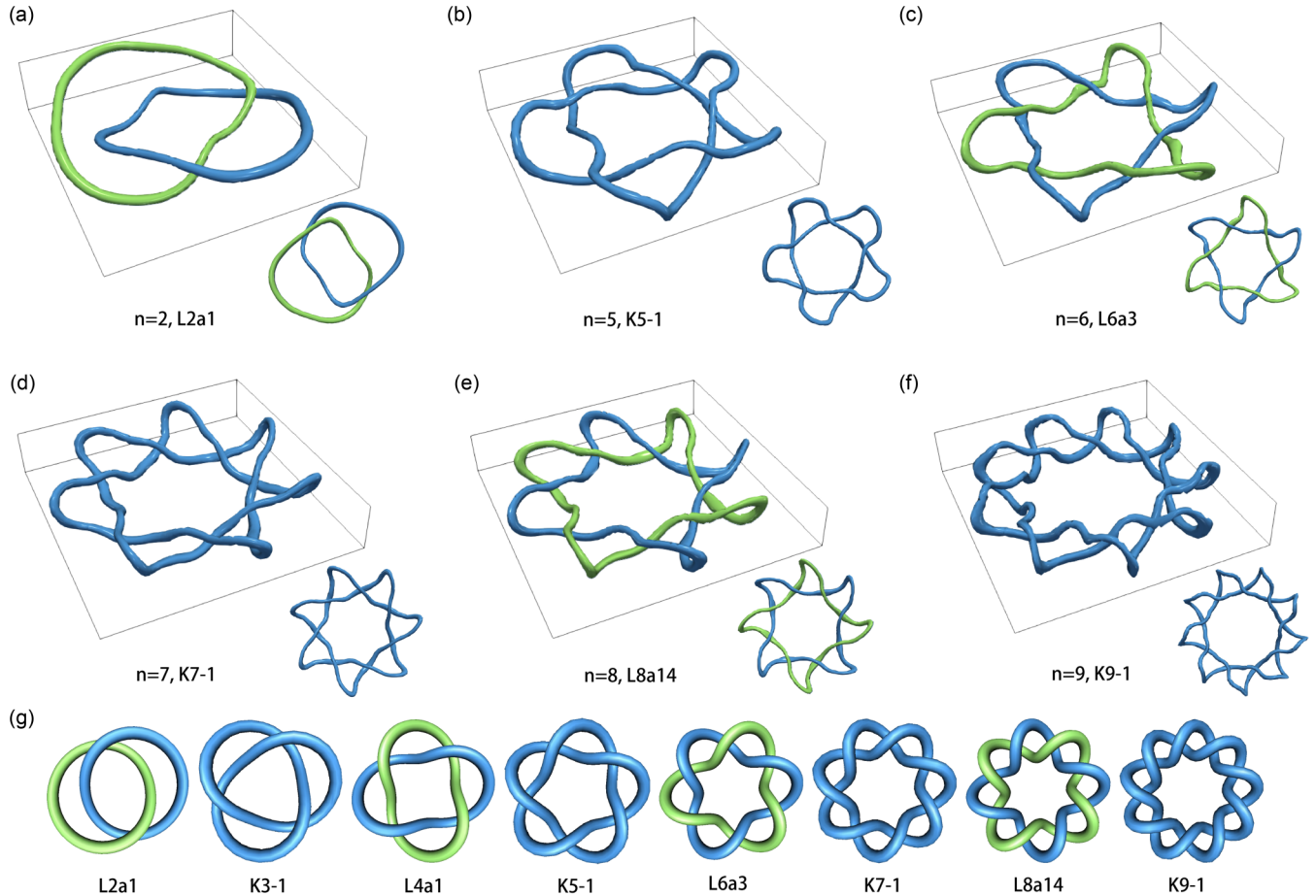


FIG. 3. Torus vortex links and knots generated with crossing number up to $n = 9$. (a) L2a1 link at $2.0t_0$. (b) K5-1 knot at $1.5t_0$. (c) L6a3 link at $t = 1.5t_0$. (d) K7-1 knot at $t = 1.5t_0$. (e) L8a14 link at $1.2t_0$. (f) K9-1 knot at $1.0t_0$. (g) Standard torus links and knots with crossing number up to 9 for KnotPlot Software configurations. All parameters are the same as those in Fig. 1, except for the Kelvin wave number, which equals the crossing number of the knots or links.

[56]). We can clearly see that the combination of the vortex rings and the reconnection of the link L4a1 occur through intermediate events with the bridge structures of four simultaneous reconnections, as shown in Figs. 2(b), 2(d), and 2(f).

C. General cases of knots and links

In our dynamic process, two types of reconnections exist: topology-changing and topology-conserving reconnections. As shown in Figs. 1(f) and 1(h) and Figs. 2(b) and 2(f), the states are topology-changing reconnections, that is, two bridge states for the transitions between different topologies. The state shown in Fig. 2(d) is classified as a topology-conserving reconnection because the before and after states are all links. The same topology can be obtained with very different geometries. In this paper, we show that for states with the same topology, the geometry is a crucial factor that determines the next step in the evolution. Although the bridge states in Figs. 1(f) and 1(h) have the same topology and reconnection mechanism, they correspond to inverse dynamical processes.

Notably, the values of the number of the reconnection points, the wave number of the Kelvin waves used to perturb the vortex rings, the crossing number, and the topological writhe of the knot and/or link generated are the same in our

cases. A general rule can thus be discerned: the type of topology generated by two perturbed rings, a knot or a link, is only determined by the parity of the wave number of the Kelvin wave perturbations, which is related to the crossing number and topological writhe of the knots or links generated. Even and odd Kelvin wave numbers applied in a pair of vortex rings can help to produce links and knots, respectively. Following this rule, we can obtain any type of torus knot or link. Examples with crossing number up to 9, except for 3 and 4, which have already been discussed, are shown in Figs. 3(a)–3(f), and the types of knots or links obtained are L2a1, K5-1, L6a3, K7-1, L8a14, and K9-1. The standard configuration of torus knots and links is shown in Fig. 3(g).

IV. DISCUSSION

A. Topological evolution of the vortices

Knots and links with high crossing numbers are much more unstable than those with low crossing numbers. As the wave number of helical Kelvin waves increases, the instability of the vortex ring itself increases [46], and the decreasing existing time of the ring, which in turn decreases the existing time of the generated knots and/or links. For $n > 6$, the created knots and/or links decay rapidly. In Ref. [57], basic

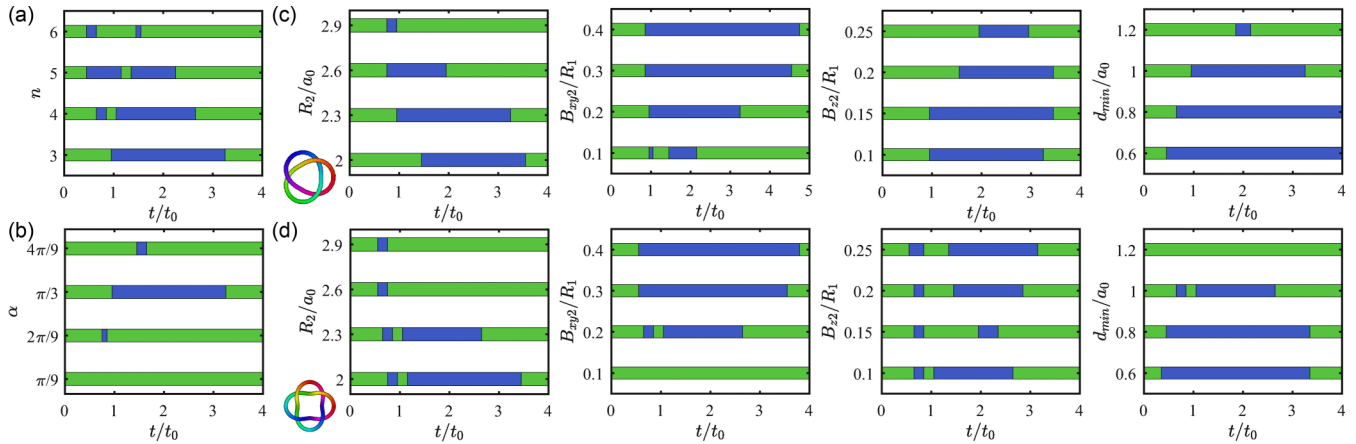


FIG. 4. (a), (b) The effect of the Kelvin wave number n and the relative angle α between the vortex rings on the topological evolution of the vortices. (c), (d) The effect of the radius of the lower ring R_2 , the radial amplitude of the Kelvin waves of the lower ring B_{xy2} , the axial amplitude of the Kelvin waves of the lower ring B_{z2} , and the initial offset between the two rings d_{\min} on the topological evolution with the wave number $n = 3$ and $n = 4$ of the initial vortex rings, respectively.

topological counting rules were developed to estimate the relative stability of frequently encountered knots and tangles. In Fig. 4(a), we show the topological transition of the vortex knots and/or links generated with crossing numbers ranging from 3 to 6. The topological transition of a trefoil knot with the initial relative angle between the two vortex rings α is shown in Fig. 4(b). Our results show that there is an ideal angle $\alpha = \pi/n$ for the generated knots and/or links with crossing number n that yields a stable state. The blue regions give the time periods when the knot and/or link survives.

It shows that the geometrical parameters of the vortices, such as macroscopic reconnection angle and concavity parameter, influence the linear momentum and energy transfers [39]. This energy transfer influences the stability of the vortex structures in turn [38,55]. In our results, the effects of other parameters, such as the initial radius of the bottom ring R_2 , the planar amplitude of the Kelvin waves B_{xy2} , the vertical amplitude of the Kelvin waves B_{z2} , and the initial offset d_{\min} on the topological transition of the generated knots and links are analyzed. The results for the trefoil knot (K3-1) are shown in Fig. 4(c) and those for the Solomon link (L4a1) in Fig. 4(d). When studying the effects of one parameter, all the others parameters are held constant. Among these parameters, by choosing an appropriate value of the initial offset d_{\min} , the topological structure we want can exist much longer, as shown in the last column in Fig. 4. In a system with a homogeneous background, the intensity of the collision of vortex rings moving toward each other depends on d_{\min} [55]. The smaller the offset is, the more violent the collision is, which induces more energy loss during the reconnection process and decreases the energy of the created topological objects. However, there is a threshold for the value of the offset that makes the reconnection of two rings possible. In Ref. [38], the energy transfer from the incompressible (kinetic) part into its compressible counterpart (density waves) during the vortex reconnection process was studied theoretically by the developed matching theory.

For the initial radii of the rings, similar values of R_1 and R_2 make reconnection easier, which results in a longer existing time of the knots and links. We found that the larger the

relative planar distortion of the rings (B_{xy}) is, the longer the existing time of the knots and links is, and the effects of vertical distortion B_z on the knots and links varied. We note that there should be a set of optimal initial parameters for generating a knot and/or link which is as stable as possible. The number of events associated with generating or breaking up knots and/or links also depends on the initial condition chosen. The possibility of links appearing is twice as high as that for knots. However, the existing time of the first appearance is quite short. To ensure that there are no connections between the vortex structures and the condensate surface for all parameters, we limit the time period to $4t_0$. Appendix B Fig. 6 and Movie1-K3-1.mp4 [56] show some long-time dynamics.

B. Length of the vortex structures

To quantify the topological evolution of the vortices, we compute the vortex length as a function of time, as shown in Fig. 5. The position of each vortex filament is found by numerically searching the minima of the density field within the condensate cloud. Then, the vortex lines are obtained by connecting these points smoothly while excluding a few isolated points induced by numerical errors. Moreover, the length of the knot and/or link can be calculated by accumulating the distance of neighbor points along the vortex line. A linked or knotted vortex structure must stretch to expand as it unties in a homogeneous system [4]. In a harmonic trap, when a vortex ring moves from a high density region toward a low density region, the radius of the ring increases gradually [53]. The variation in length reflects the complex interacting process of vortex structures in a harmonic trap. During the untying process of knots and links, the length of these structures increases. However, the decrease in the vortex length during the formation of knots and links is not obvious because this length also increases when these structures move toward the edge of the condensate cloud. A recent study [43] observed the boundary effects on vortex dynamics that allow double reconnections, rebounds, and ejections of vortex lines in a cigar-shaped atomic BEC in addition to

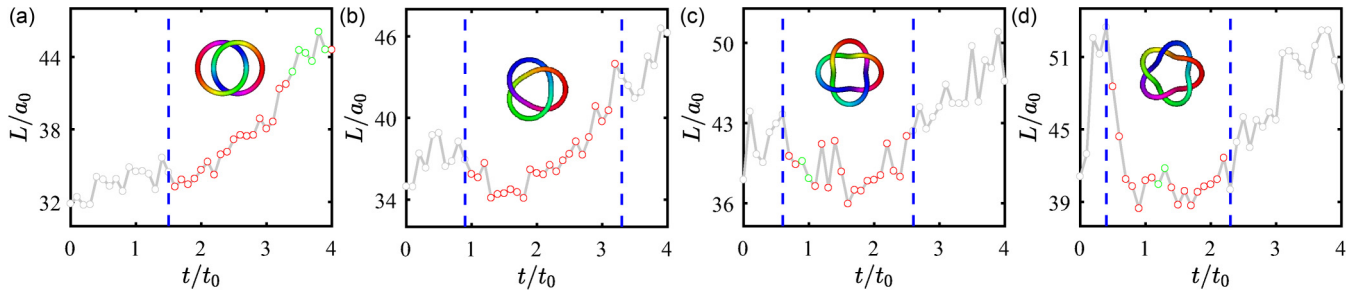


FIG. 5. Length L of the vortex structures as a function of time t in a harmonic trap BEC. (a)–(d) A trivial link is perturbed by Kelvin waves with wave numbers $n = 2, 3, 4, 5$, respectively. The dashed blue lines indicate the transitions between different topologies. The red open circles indicate the time period when a knot and/or link (colored patterns) can be clearly identified, and the green circles represent the topology-conserving reconnections.

standard reconnections in infinite uniform fluids. Between different topologies, the lengths of vortex structures, except for topology-conserving intermediate structures, vary considerably.

C. Pathways of topological transitions

In the above discussions, the initial vortex rings are all coaxial, and all the reconnections at different points on the vortex rings occur simultaneously, which results in rings-knot-rings and rings-link-rings transitions. However, the simultaneous reconnections do not affect the intrinsic physics; that is, a transition can develop in both directions between a complex topology and a simple topology in a confined system. In Appendix C, we show that by further deforming the

initial rings or changing their relative positions, the sequence of reconnection events can be controlled. New pathways of the topology transition are provided, such as rings-link-knot-link-rings and rings-link-ring-link-rings, through successive reconnections, even though the wave number of the Kelvin perturbations n is odd (Appendix C Figs. 7 and 8), which provides further evidence of the transition between a simple topology and a complex topology in both directions.

V. CONCLUSION

In conclusion, we find that torus vortex knots and links can be generated through reconnection of vortex rings in a confined superfluid BEC. Kelvin wave perturbations played synergistic roles in forming and stabilizing vortex knots and

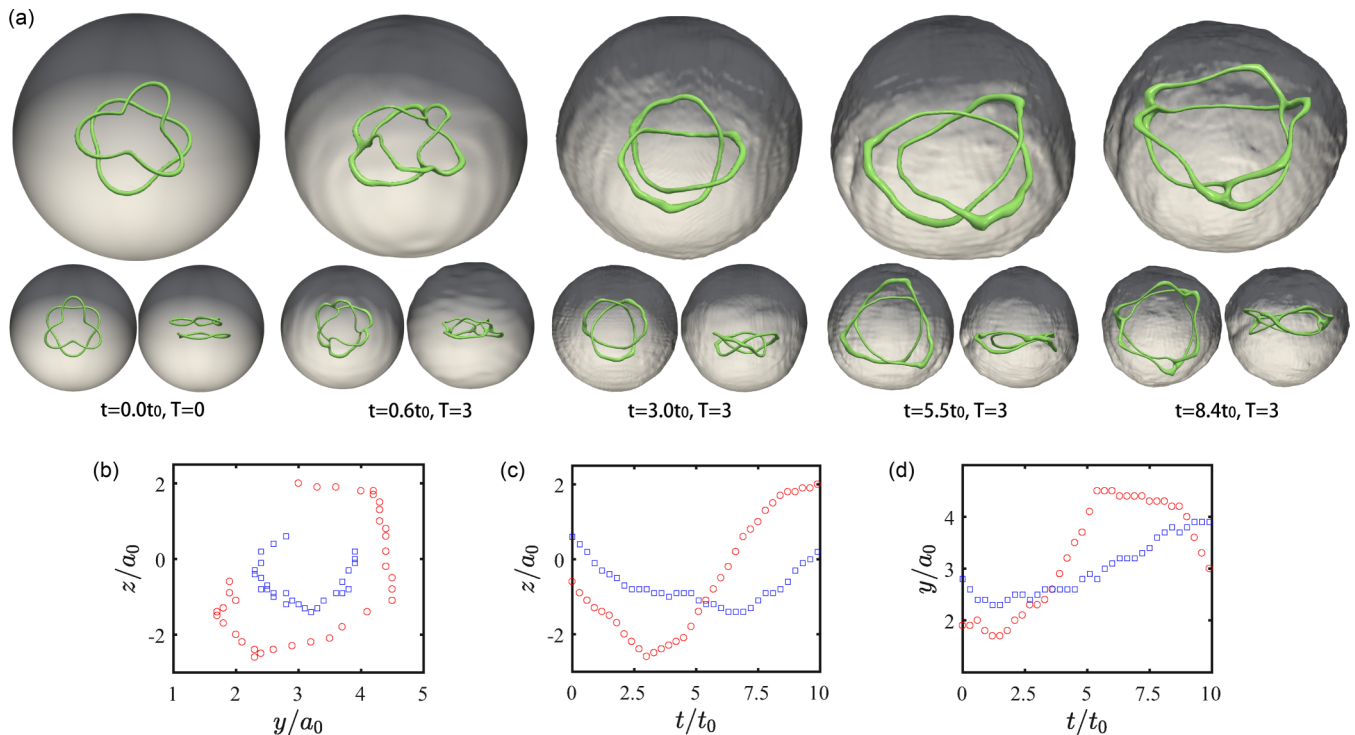


FIG. 6. Generation of a trefoil vortex knot in a spherical condensate. (a) Five successive snapshots with top views and side views that show the dynamics of trivial links for Kelvin wave number $n = 3$. T is the irreducible contribution to the helicity originating from the global vortex topology. (b)–(d) Trajectories of two vortex points in the half yOz plane ($y > 0$).

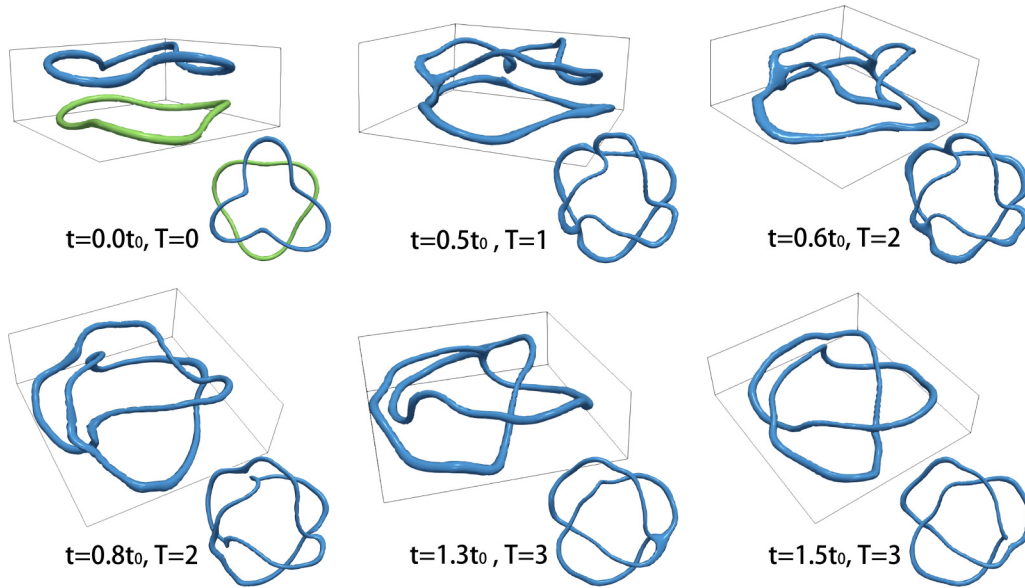


FIG. 7. Rings-link-knot dynamics in a spherical condensate. Six successive snapshots show the dynamics of trivial links for Kelvin wave number $n = 3$. The top ring is initially distorted by a dimensionless strength of 0.3 to overcome the periodic Kelvin wave perturbations.

links in this process. Notably, even Kelvin wave numbers produced links and odd Kelvin wave numbers produced knots. We show the dependence of the stability of the generated knots and links on the various parameters of the system. The initial relative angle of the two vortex rings is crucial for the knots and links to survive for a long time. The critical value of the relative angle is π/n . The variation of the vortex length during the topological evolution is calculated, and the tendency of which coincides with the results in Ref. [4]. Mostly, vortex knots and links untied monotonically, which simplified their topology at each step [1,2,26]. However, in classical and

superfluid turbulent tangle, structures with simple topologies can form complex vortex structures [9,29,37,58]. But this process is not reproducible and controllable. In a trapped system, the transition between trivial and complex topologies occurs in both directions while the knot and/or link comes and goes in the course of time.

In the main text, we discussed the evolution of the vortices in systems with a harmonic trap. In Appendixes D and E, we also show that all these results can be achieved in BEC systems with box-trapping potentials or with periodic boundary conditions. The simplicity and robustness of our

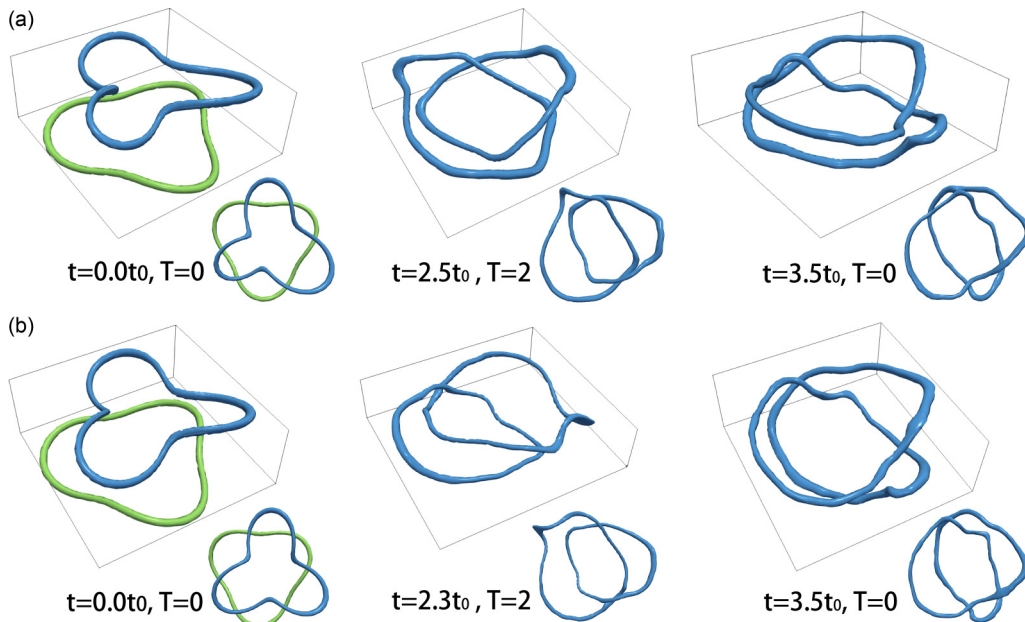


FIG. 8. Rings-link-ring dynamics in a spherical condensate. Three successive snapshots show dynamics of trivial links with Kelvin wave number $n = 3$. (a) The top ring is initially distorted by a dimensionless strength 0.5. (b) The top ring is displaced away from the trap center over a dimensionless distance 0.5 in the y direction.

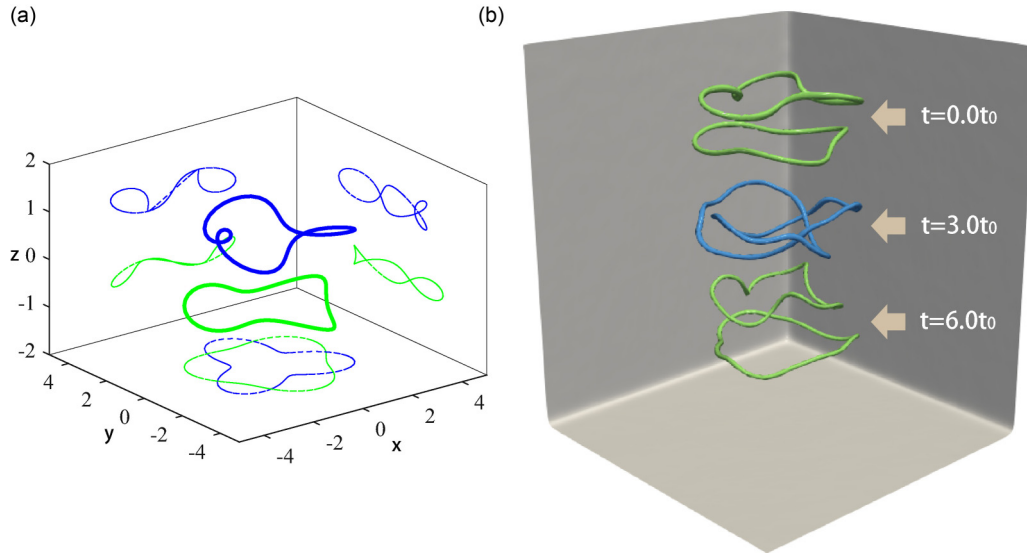


FIG. 9. Dynamics of vortex structures with box potential. (a) Initial condition of two vortex rings (thick blue and green lines) with Kelvin wave perturbations $n = 3$ and box potential. The dotted blue and green lines are the projections to the xOy , xOz , and yOz planes. (b) Three typical isosurfaces of the vortex structures at time $t = 0, 3.0t_0, 6.0t_0$, which show the trivial link, knot, and trivial link evolution. The parameters used are the same as those in Fig. 1 in the main text.

method provides a framework for discovering knots and links with complex topologies, which might be of great interest in the strategic design of topologically complex structures with chemical and biological molecules, and in understanding the evolution and mechanisms of confined turbulent systems.

ACKNOWLEDGMENTS

We acknowledge funding by the National Science Foundation of China under Grants No. 11775178, No. 11947301, and No. 61835013, by National Key R&D Program of China under Grant No. 2016YFA0301500, the Strategic Priority Research Program of the Chinese Academy of Sciences under Grants No. XDB01020300 and No. XDB21030300, the Major Basic Research Program of Natural Science of Shaanxi Province under Grants No. 2017KCT-12 and No. 2017ZDJC-32. This research is also supported by the Double First-Class University Construction Project of Northwest University.

APPENDIX A: HELICITY

As the only other known quadratic invariant besides energy, helicity has important significance for an ideal classical fluid in three dimensions. It is generally accepted that helicity is composed of several contributions among which internal (or intrinsic) twist makes up an important component. However, it is not obvious how a structureless vortex filament can acquire an internal twist contribution [36]. In our systems, we only consider the centerline helicity because a twist requires additional information about the fine structure of the vortex core, which is challenging to obtain experimentally [2,4]. Thus, the centerline helicity is given by

$$H_c = \Gamma^2 \left(\sum_{i \neq j} Lk_{ij} + \sum_i W_{r_i} \right), \quad (\text{A1})$$

where Lk_{ij} is the linking number between vortex lines i and j , W_{r_i} is the 3D writhe of line i , which includes contributions from knotting in addition to helical coils. The circulation of vortices is quantized and given by $\Gamma = \oint_C \mathbf{v}(\ell) d\ell = 4\pi\hbar/(2m)$, where \mathbf{v} is the flow velocity. There is an irreducible contribution T to the helicity H_c that originates from the global vortex topology, which is not removable, even by the long-scale smoothing of the length of the vortex filament [2,4]. This effective knotting and/or linking number with integer values can be used to identify the transfer of helicity across scales between knots and/or links and helically distorted coils through reconnection events. In Figs. 6–8, we show the value

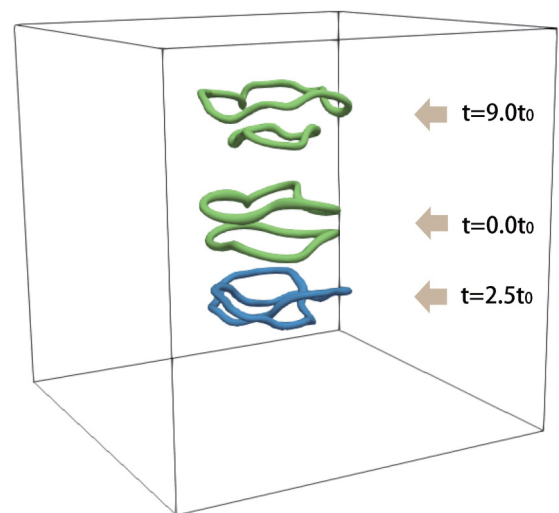


FIG. 10. Dynamics of vortex structures under periodic boundary conditions. Three typical isosurfaces of the vortex structures at time $t = 0, 2.5t_0, 9.0t_0$, which show the trivial link, knot, and trivial link evolution. The parameters used are the same as those in Fig. 1 in the main text.

of T at some typical time steps during the formation process of two perturbed vortex rings with Kelvin wave number $n = 3$. The value of T can also be used to identify topology-changing and topology-conserving reconnections.

APPENDIX B: OSCILLATION OF A TREFOIL KNOT

Considering the oscillatory nature of a vortex ring in a harmonically trapped condensate, we expect the structures generated through the reconnections of two rings to also oscillate in the condensate cloud, which makes the existing time of the knots and/or links longer. As mentioned in the main text, there is a set of optimum initial parameters that makes the existing time of the knots and/or links much longer than that of other structures. As shown in Fig. 6, the movement of the vortex structures can last up to $8.4t_0$ without connections with the condensate surface. We provide five typical snapshots of the density isosurface during the formation and dissolution of trefoil knots. For the given initial parameters, the trefoil that appears initially survives from $0.7t_0$ to $8.3t_0$. We can track the trajectory of the two vortex points in the half yOz plane with ($y > 0$), as shown in Fig. 6(b). Figures 6(c) and 6(d) show the evolution of the positions of the two vortex points over time in the z and y directions, respectively. The relative positions of these two points continually change and they exchange their positions occasionally. This type of movement in the entire space provides a source for reconnection and separation events. We show the evolution of the system from $t = 0$ to $15t_0$ in Supplemental Movie1-K3-1.mp4 [56], which displays the Rings-Knot-Rings-Knot-Rings oscillation clearly.

APPENDIX C: SUCCESSIVE RECONNECTIONS

In the main text, the initial conditions we chose are highly symmetric, which reflects the physics of the reconnections of the two vortex rings. However, the conditions for creating knots and/or links via the reconnection of two perturbed vortex rings are not highly restrictive. For the initial conditions set in the main text, all reconnections at different points on the two rings occur simultaneously because the deformation of the rings induced by Kelvin waves is periodic and there are no fluctuations in the system. If we introduce extra distortions that change the amplitude of deformation at different nodes of the top vortex ring, as shown in Fig. 7 ($t = 0$), the process involving the periodic change in the shape of the vortex ring is disrupted. Then the reconnections can occur successively in time. After the first two reconnections are complete, an L2a1 link emerges at $0.8t_0$, followed by another reconnection at $1.3t_0$. A trefoil knot arises after the third reconnection at $1.5t_0$, and it turns into a link and then two rings through successive reconnections in the subsequent dynamic process. Because the resolution of the complex topology (trefoil knot in this case) is just the reverse of the formation process and follows similar untying dynamics as those in Ref. [4], we do not show it in Fig. 7. By adjusting the initial deformation of the top vortex ring, rings-link-knot-link-rings dynamics are successfully achieved in our confined system, which again demonstrates that the evolution between a simple topology and a complex topology can develop in both directions. We

note that due to the inhomogeneous density distribution of the harmonically trapped condensate, the complete loop of rings to rings may be disrupted at any stage by the connections of the vortices with the condensate surface. If we shift the relative initial positions of the two vortex rings to make them slightly noncoaxial, the same results can be obtained as those yielded by adjusting the deformation.

Strong additional asymmetric deformation and the large noncoaxial displacement of the vortex rings can provide new pathways for topology transitions. In Fig. 8(a), we show the results of applying stronger additional deformation to the top vortex ring rather than that applied in Fig. 7(a). An L2a1 link emerges at $2.5t_0$ after two successive reconnections, and this link turns into a ring through another reconnection at $3.5t_0$. The same things occur when we displace the center of the top vortex ring away from the z axis by $5a_0$, as shown in Fig. 8(b). In these two cases, a topology transfer process, rings-link-ring-link-rings, is observed. As in Fig. 7, we only show the first half of the dynamic process. As described in Refs. [2,31], the stepwise simplification during DNA untying or vortex knots and/or links dissolution in viscous fluids for an L2a1 linked configuration (a K3-1 knotted configuration) should follow the link-ring-rings pathway (knot-link-ring-rings) with decreasing crossing numbers.

APPENDIX D: BOX POTENTIAL

To verify the mechanism of achieving transitions from a simple topology to a complex one is not affected by the boundary conditions, we also performed calculations with the box potential and they yielded similar results. We employ a box potential in the form

$$V_{\text{box}}(\mathbf{r}) = \begin{cases} V_0, & |x|, |y|, |z| = 7.5a_0 \\ 0, & |x|, |y|, |z| < 7.5a_0, \end{cases} \quad (\text{D1})$$

with potential height V_{box} to replace V_{tr} in the GP equation in the main text. The size of the system remains $151 \times 151 \times 151$. This substitution can be experimentally achieved using two digital micromirror devices [59]. By loading 9×10^5 atoms into a trap, a cubic density profile is produced. Figure 9(a) shows the initial state of a pair of unlinked vortex rings with Kelvin wave perturbations in the box potential. The parameters are the same as those used in the harmonic trap for creating a trefoil K3-1 knot (Fig. 1 in the main text). In Fig. 9(b), three typical time sequences illustrate the initial state, trefoil knot, and trivial link during the dynamic process. The topology transition of rings-knot-rings is the same as that in a harmonic trap (Supplemental Movie3-K3-1box.mp4 [56]). For Kelvin wave number $n = 4$, we can also repeat the rings-link-rings transition (Supplemental Movie4-L4a1box.mp4 [56]). Moreover, for successive reconnections, we can achieve rings-link-knot-link-rings and rings-link-ring-link-rings dynamics.

APPENDIX E: PERIODIC BOUNDARY CONDITIONS

We also checked the results of the systems with periodic boundary conditions. We demonstrated that for sufficiently close leapfrogging vortex rings with perturbed Kelvin waves on them, a series of reconnections can happen, and a

topologically more complex vortex structure can be created in an unbounded domain. To ensure that the phase matches across periodic boundaries, a constant gradient should be

added [2]. The topological evolution from a trivial link to a trefoil in a system with a periodic boundary condition is demonstrated as shown in Fig. 10.

-
- [1] D. Kleckner, M. Scheeler, and W. Irvine, *Nat. Phys.* **9**, 253 (2013).
- [2] M. W. Scheeler, D. Kleckner, D. Proment, G. L. Kindlmann, and W. T. M. Irvine, *Proc. Natl. Acad. Sci.* **111**, 15350 (2014).
- [3] I. Shomroni, E. Lahoud, S. Levy, and J. Steinhauer, *Nat. Phys.* **5**, 193 (2009).
- [4] D. Kleckner, L. H. Kauffman, and W. T. M. Irvine, *Nat. Phys.* **12**, 650 (2016).
- [5] D. S. Hall, M. W. Ray, K. Tiurev, E. Ruokokoski, A. H. Gheorghie, and M. Möttönen, *Nat. Phys.* **12**, 478 (2016).
- [6] F. Maucher, S. A. Gardiner, and I. G. Hughes, *New J. Phys.* **18**, 063016 (2016).
- [7] D. Proment, M. Onorato, and C. F. Barenghi, *Phys. Rev. E* **85**, 036306 (2012).
- [8] D. Proment, M. Onorato, and C. F. Barenghi, *J. Phys.: Conf. Ser.* **544**, 012022 (2014).
- [9] H. Aref and I. Zawadzki, *Nature* **354**, 50 (1991).
- [10] H. K. Moffatt, *Proc. Natl. Acad. Sci.* **111**, 3663 (2014).
- [11] R. L. Ricca and M. A. Berger, *Phys. Today* **49**, 28 (1996).
- [12] D. M. Raymer and D. E. Smith, *Proc. Natl. Acad. Sci.* **104**, 16432 (2007).
- [13] U. Tkalec, M. Ravnik, S. Čopar, S. Žumer, and I. Muševič, *Science* **333**, 62 (2011).
- [14] A. Martínez, M. Ravnik, B. Lucero, R. Visvanathan, S. Žumer, and I. I. Smalyukh, *Nat. Mater.* **13**, 258 (2014).
- [15] S. Wasserman and N. Cozzarelli, *Science* **232**, 951 (1986).
- [16] T. Schlick and W. K. Olson, *Science* **257**, 1110 (1992).
- [17] H. Dongran, P. Suchetan, L. Yan, and Y. Hao, *Nat. Nanotechnol.* **5**, 712 (2010).
- [18] K. S. Chichak, S. J. Cantrill, A. R. Pease, S.-H. Chiu, G. W. V. Cave, J. L. Atwood, and J. F. Stoddart, *Science* **304**, 1308 (2004).
- [19] D. W. Sumners, *Notices AMS* **42**, 528 (1995).
- [20] K. Shimokawa, K. Ishihara, I. Grainge, D. J. Sherratt, and M. Vazquez, *Proc. Natl. Acad. Sci.* **110**, 20906 (2013).
- [21] D. Liu, Y. Shao, G. Chen, Y.-C. Tse-Dinh, J. A. Piccirilli, and Y. Weizmann, *Nat. Commun.* **8**, 14936 (2017).
- [22] R. S. Forgan, J.-P. Sauvage, and J. F. Stoddart, *Chem. Rev.* **111**, 5434 (2011).
- [23] V. Marcos, A. J. Stephens, J. Jaramillo-Garcia, A. L. Nussbaumer, S. L. Woltering, A. Valero, J.-F. Lemonnier, I. J. Vitorica-Yrezabal, and D. A. Leigh, *Science* **352**, 1555 (2016).
- [24] J. J. Danon, A. Krüger, D. A. Leigh, J.-F. Lemonnier, A. J. Stephens, I. J. Vitorica-Yrezabal, and S. L. Woltering, *Science* **355**, 159 (2017).
- [25] Y. Segawa, M. Kuwayama, Y. Hijikata, M. Fushimi, T. Nishihara, J. Pirillo, J. Shirasaki, N. Kubota, and K. Itami, *Science* **365**, 272 (2019).
- [26] M. W. Scheeler, W. M. van Rees, H. Kedia, D. Kleckner, and W. T. M. Irvine, *Science* **357**, 487 (2017).
- [27] M. R. Dennis, R. P. King, B. Jack, K. O'Holleran, and M. J. Padgett, *Nat. Phys.* **6**, 118 (2010).
- [28] S. J. Tempone-Wiltshire, Shaun P. Helmerson, and K. Johnstone, *Sci. Rep.* **6**, 24463 (2016).
- [29] C. F. Barenghi, *Milan J. Math.* **75**, 177 (2007).
- [30] X. Liu and R. L. Ricca, *Sci. Rep.* **6**, 24118 (2016).
- [31] R. Stolz, M. Yoshida, R. Brasher, M. Flanner, K. Ishihara, D. J. Sherratt, K. Shimokawa, and M. Vazquez, *Sci. Rep.* **7**, 12420 (2017).
- [32] S. Zuccher and R. L. Ricca, *Phys. Rev. E* **95**, 053109 (2017).
- [33] A. Vilhois, D. Proment, and G. Krstulovic, *Phys. Rev. Fluids* **2**, 044701 (2017).
- [34] T. T. Lim and T. B. Nickels, *Nature* **357**, 2225 (1992).
- [35] J. Koplik and H. Levine, *Phys. Rev. Lett.* **76**, 4745 (1996).
- [36] H. Salman, *Proc. R. Soc. A* **473**, 20160853 (2017).
- [37] A. Vilhois, D. Proment, and G. Krstulovic, *Phys. Rev. E* **93**, 061103(R) (2016).
- [38] D. Proment and G. Krstulovic, *Phys. Rev. Fluids* **5**, 104701 (2020).
- [39] A. Vilhois, D. Proment, and G. Krstulovic, *Phys. Rev. Lett.* **125**, 164501 (2020).
- [40] V. Bretin, P. Rosenbusch, F. Chevy, G. V. Shlyapnikov, and J. Dalibard, *Phys. Rev. Lett.* **90**, 100403 (2003).
- [41] A. L. Fetter, *Phys. Rev. A* **69**, 043617 (2004).
- [42] D. Kivotides, J. C. Vassilicos, D. C. Samuels, and C. F. Barenghi, *Phys. Rev. Lett.* **86**, 3080 (2001).
- [43] S. Serafini, L. Galantucci, E. Iseni, T. Bienaimé, R. N. Bisset, C. F. Barenghi, F. Dalfovo, G. Lamporesi, and G. Ferrari, *Phys. Rev. X* **7**, 021031 (2017).
- [44] A. L. Fetter and A. A. Svidzinsky, *J. Phys.: Condens. Matter* **13**, R135 (2001).
- [45] C. F. Barenghi, R. Hänninen, and M. Tsubota, *Phys. Rev. E* **74**, 046303 (2006).
- [46] J. L. Helm, C. F. Barenghi, and A. J. Youd, *Phys. Rev. A* **83**, 045601 (2011).
- [47] H. K. Moffatt, *J. Fluid Mech.* **35**, 117 (1969).
- [48] A. J. Niemi, *Phys. Rev. Lett.* **94**, 124502 (2005).
- [49] C. E. Laing, R. L. Ricca, and D. W. L. Sumners, *Sci. Rep.* **5**, 9224 (2015).
- [50] M. Vazquez and D. W. Sumners, *Math. Proc. Cambridge Philos. Soc.* **136**, 565 (2004).
- [51] L. Galantucci, A. W. Baggaley, N. G. Parker, and C. F. Barenghi, *Proc. Natl. Acad. Sci.* **116**, 12204 (2019).
- [52] <http://katlas.org>.
- [53] B. Jackson, J. F. McCann, and C. S. Adams, *Phys. Rev. A* **61**, 013604 (1999).
- [54] W.-K. Bai, J.-c. Xing, T. Yang, W.-L. Yang, and W.-M. Liu, [arXiv:1906.04020](https://arxiv.org/abs/1906.04020).
- [55] M. Leadbeater, T. Winiecki, D. C. Samuels, C. F. Barenghi, and C. S. Adams, *Phys. Rev. Lett.* **86**, 1410 (2001).
- [56] See Supplemental Material at <http://link.aps.org/supplemental/10.1103/PhysRevA.102.063318> for movies.
- [57] V. P. Patil, J. D. Sandt, M. Kolle, and J. Dunkel, *Science* **367**, 71 (2020).
- [58] H. K. Moffatt and R. L. Ricca, *Proc. R. Soc. London A* **439**, 411 (1992).
- [59] L. Baird, X. Wang, S. Roof, and J. E. Thomas, *Phys. Rev. Lett.* **123**, 160402 (2019).